

# A Network Science Approach to Granular Time Series Segmentation

Ivana Kesić<sup>a</sup>, Carolina Fortuna<sup>a</sup>, Mihael Mohorčič<sup>a</sup>, Blaž Bertalanšč<sup>a</sup>

<sup>a</sup>*Jozef Stefan Institute, Department of Communication Technologies, Jamova 39, 1000, Ljubljana, Slovenia*

---

## Abstract

Time series segmentation (TSS) is one of the time series (TS) analysis techniques, that has received considerably less attention compared to other TS related tasks. In recent years, deep learning architectures have been introduced for TSS, however their reliance on sliding windows limits segmentation granularity due to fixed window sizes and strides. To overcome these challenges, we propose a new more granular TSS approach that utilizes the Weighted Dual Perspective Visibility Graph (WDPVG) TS into a graph and combines it with a Graph Attention Network (GAT). By transforming TS into graphs, we are able to capture different structural aspects of the data that would otherwise remain hidden. By utilizing the representation learning capabilities of Graph Neural Networks, our method is able to effectively identify meaningful segments within the TS. To better understand the potential of our approach, we also experimented with different TS-to-graph transformations and compared their performance. Our contributions include: a) formulating the TSS as a node classification problem on graphs; b) conducting an extensive analysis of various TS-to-graph transformations applied to TSS using benchmark datasets from the TSSB repository; c) providing the first detailed study on utilizing GNNs for analyzing graph representations of TS in the context of TSS; d) demonstrating the effectiveness of our method, which achieves an average F1 score of 0.97 across 59 diverse TSS benchmark datasets; e) outperforming the seq2point baseline method by 0.05 in terms of F1 score; and f) reducing the required training data compared to the baseline methods.

*Keywords:* time series, time series segmentation, graph neural networks, graphs, transformations

---

## 1. Introduction

In today's digital era, time series (TS) are one of the most frequently encountered data types. Low-cost, high-resolution sensors have become a key part in mobile devices, industrial monitoring and healthcare, producing large amounts of TS data that capture the temporal patterns and essential statistical properties of various processes or phenomena [1]. With the rapid progress in automatic data acquisition and storage, we are now faced with the challenge of data that far exceeds our comprehension. TS analysis methods such as clustering, classification or regression, are therefore essential for effective and efficient processing of TS data [2, 3, 4, 5]. Although these methods are crucial, they often benefit from first segmenting the TS into smaller, more manageable parts, through a process known as Time Series Segmentation (TSS). It first involves *identifying critical time points dividing* the TS into smaller segments and second *label them based on activity*. This segmentation step can significantly simplify subsequent

tasks such as classification or anomaly detection and provide more targeted insights. For example, in the field of telecommunications [6] the increasing volume of the network traffic data is a constant challenge. With TSS, we can segment network traffic, making it easier to detect patterns and respond swiftly to potential issues, such as peak usage periods, while optimizing bandwidth efficiency.

In recent years, deep learning (DL) [7, 8] architectures have been introduced as a TSS method, however they have not yet reached the same level of performance in TSS as in other fields such as computer vision. Many of these approaches rely on sliding-window techniques, where the TS is partitioned into evenly sized segments that are individually labeled before being recombined. While sliding-window methods yield satisfactory results, they limit the granularity of segmentation due to fixed window sizes and strides.

A different, less mainstream approach to TS analysis, explores graphs as a viable TS representation [9, 10, 11, 12] where each value in the raw TS is represented as a node. Transforming TS into graphs not only preserves the temporal order of the data, but also reveal interactions and dependencies between non consecutive points, which is important for tasks such as TSS. This transformation enables the adoption of Graph Neural Networks (GNNs), which are particularly well-suited to learn complex structural features. GNNs can help identify the critical transition points that distinguish different segments, and are able to capture subtle temporal dependencies and variations that often precede significant changes in the TS. Such representations based on node density and message passing between node neighborhoods naturally eliminate the fixed window sizes and strides from DL.

By considering the combination of TS graph representations and GNNs, and taking inspiration from the dense labeling approach in computer vision where every pixel is assigned a class label [13], we can reformulate the TSS challenge as a node-level classification problem. In our graph representation of TS data, dense labeling entails assigning a specific label to each node, ensuring that even the most subtle transitions are detected and appropriately classified. In this work we aim to conduct a comprehensive and robust exploration of the different graph representations for TSS on the TSSB benchmark datasets in combination with GNNs. Based on the findings of this exploration, we propose a new approach that combines the Weighted Dual Perspective Visibility Graph (WDPVG) transformation with a GAT-based GNN architecture. The contributions of this paper are as follows:

- We formulate the TSS as a node classification problem on graphs
- We perform an extensive study on the suitability of several TS to graph transformations for TSS on TSSB benchmark datasets
- We perform a first-time analysis of TS graph representation for TSS with GNNs
- We show that our proposed approach achieves an average F1 score of 0.97 on 59 different open source TSS benchmark datasets from different domains
- We show that our proposed method outperforms the baseline seq2point method by 0.05 in F1 score

- We show that the proposed method requires significantly less training data for training compared to the baseline.

This paper is organized as follows. The related work is discussed in Section 2. Section 3 provides the problem formulation, while Section 4 elaborates on the proposed time series transformation. Section 5 introduces the proposed deep learning architecture, Section 6 describes the relevant methodological and experimental details, while Section 7 provides thorough analysis of the results. Finally, Section 8 concludes the paper.

## 2. Related work

Time series segmentation is an area of research in the TS analysis field, which received less attention compared to the other related TS tasks. However, its importance is emphasized by its application in various domains, such as healthcare, finance, energy, traffic and networking. We can divide it into three main categories depending on its application: Change Point Detection (CPD)[14][15][16], Windowed Segment Classification (WSC)[7] and Dense Labeling or Precise Segmentation (DLPS)[17]. An example of the three approaches can be found in Figure 1, where Figure 1a) shows the ground truth TS example with 4 different segments, Figure 1b) shows the output of the CPD method, Figure 1c) shows the output of the WSC segmentation and the last Figure 1d) shows the DLPS segmentation.

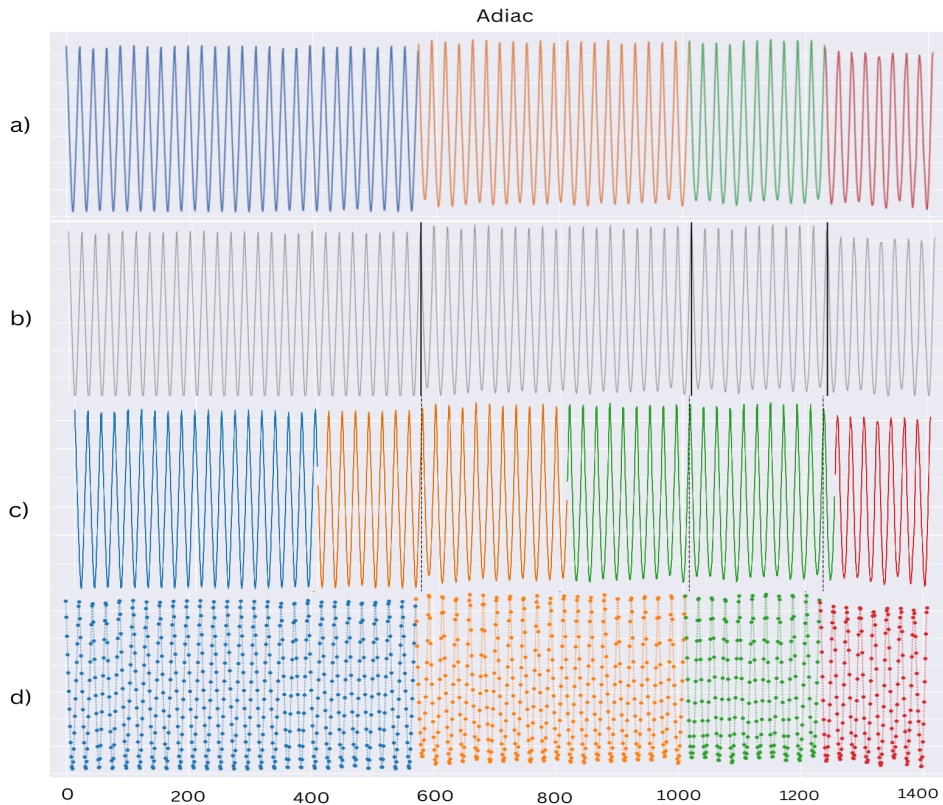


Figure 1: Example of three existing segmentation categories for the Adiac TSSB dataset. a) Ground truth, b) CPD, c) WSC, d) DLPS

Early research predominantly concentrated on identifying boundaries where abrupt changes occur, known as Change Points (CPs). Arif et al. [15] analyzed 25 years of Malaysian climate data to identify significant shifts in climate patterns. Their methodology employed two statistical techniques: Cumulative SUM (CUSUM) to detect shifts and bootstrapping to confirm the significance of those shifts. In contrast, Ermshaus et al.[14] treated CPD primarily as a preprocessing step for TSS. Their hierarchical approach recursively partitions a univariate time series into two segments. For each potential split point, a binary k-NN classifier is trained, and the split point yielding the highest accuracy is selected as the change point. ClaSP[14] further automates this process by determining hyperparameters from the data through self-supervision and specialized algorithms, thus removing the need for manual parameter tuning. Because traditional CPD methods often struggle with subtle changes in autocorrelation structures and may exhibit high false-alarm rates, De Ryck et al.[18] addressed these challenges by employing a deep learning autoencoder. Their approach learns a time-invariant representation of the time series, focusing on stable features across the data. To detect change points, they calculate a dissimilarity measure based on Euclidean distances between consecutive windows' feature representations. Notable increases in this measure indicate potential change points.

However, a key limitation of CPD lies in its inability to classify the underlying nature of each segment. Consequently, TSS has evolved into a classification problem to overcome this gap. The most common strategy is WSC, in which the time series is split into fixed-length windows, each labeled independently. For instance, Perslev et al.[7] employed a CNN-based U-Time architecture to segment sleep stages in EEG signals. A drawback, however, is that segmentation granularity depends on the chosen window size. Reducing the window to a single time stamp yields the most granular approach, referred to as DLPS. Gaugel et al.[17] introduced a deep learning model that merges sliding window and dense labeling techniques by employing CNNs for intra-window feature extraction, LSTM networks for inter-window contextual understanding, and a refinement module for dense labeling. Evaluated on multivariate time series with their model achieved a segmentation accuracy of approximately 96%.

Compared to the presented related work, despite notable similarities, majority of the works focus on the CPD, while DLPS is mostly done on multivariate TS. To the best of our knowledge, this work is the first formulating the segmentation of univariate TS data as DLPS, through the graph dimensionality expansion representation of TS and GNNs.

### 3. Problem formulation

TSS as a fundamental task in time series analysis involves partitioning a sequence into semantically meaningful segments. In this work, we formulate TSS as a point-wise classification problem, also referred to as DLPS, where each time step in a time series is assigned a categorical label indicating its segment membership. This formulation aligns well with graph node classification tasks [19]. By representing the TS as a graph, where each time point corresponds to a graph node, the task of segmenting the series translates to assigning labels to these nodes.

Let  $S$  be a univariate time series of length  $N$ :

$$S = \{s_1, s_2, \dots, s_N\}, \quad s_i \in \mathbb{R} \quad (1)$$

where each  $s_i$  represents a value of the TS at time step  $i$ . The objective of TSS is to assign a label  $y_i$  to each time point  $s_i$ , where the label corresponds to one of  $C$  predefined segment classes:

$$Y = \{y_1, y_2, \dots, y_N\}, \quad y_i \in \{0, 1, \dots, C\} \quad (2)$$

To assign the labels, we first construct a corresponding TS graph representation through a transformation function  $T(S)$ , i.e.,  $G = T(S)$ . The resulting graph  $G = (V, E)$  encapsulates the link dynamics of TS  $S$ , where:

- $V = \{v_1, v_2, \dots, v_N\}$  is the set of nodes, where each node  $v_i$  represents a time step  $s_i$ .
- $E \subseteq V \times V$  is the set of edges that define the structural relationships between time points.

Given the graph  $G$ , the goal of TSS is to assign a segment label  $y_i$  to each node (i.e., time step). The segmentation task is then defined as node classification function  $F_G$  over the graph:

$$y_i = F_G(G; \theta)_i \quad (3)$$

where  $\theta$  represents the model parameters. This formulation aims to provide continuous and dense labeling across all time steps, enabling fine-grained segmentation.

#### 4. Time series to graph transformations

In this section, we describe the main data preparation step, how to transform TS into graphs. We define the transformation  $T()$  that transforms the input TS  $S$  to its corresponding graph  $G$ :  $G = T(S)$ . Each node in the graph corresponds to a time stamp in the TS, while the edges between them represent their relationships. To determine the set of edges, Silva et al.[20] collected and presented three classes of approaches according to the underlying mapping concepts: the Visibility Graph Transformations, the Transition Networks and the Proximity Networks. Table 1 provides a comparative overview of these transformation methods. The first column lists all the variants that were utilised in this work. The second column specifies the node representation used in each algorithm, where  $t$  denotes time points, while  $q_i$ ,  $\pi_i$  or  $\bar{z}_i$  correspond to state based representations of the time points. The third column describes the edge type, such as Natural Visibility (NV) and Horizontal Visibility (HV) edges in Visibility Networks, Transition Probability (TP) edges indicating probability based connections, and Distance based Measure (DM) edges in Proximity Networks. The fourth and fifth columns indicate whether the generated networks have directed and weighted edges.

	<b>Network type</b>	<b>node</b>	<b>edge</b>	<b>directed</b>	<b>weighted</b>
<b>VISIBILITY</b>	Natural Visibility Graph (NVG)	t	NV	×	×
	Horizontal Visibility Graph (HVG)	t	HV	×	×
	Directed NVG	t	NV	✓	×
	Directed HVG	t	HV	✓	×
	Weighted NVG	t	NV	✓	✓
	Weighted HVG	t	HV	✓	✓
	Weighted Dual Perspective Visibility Graph	t	NV	✓	✓
	<b>TRANSITION</b>	Quantile Network	$q_i$	TP	✓
Ordinal Partition Transition Network		$\pi_i$	TP	✓	✓
Coarse-Grained Phase Space Graph		$\vec{z}_i$	TP	✓	✓
<b>PROXIMITY</b>	k-NN Network	$\vec{z}_i$	DM	✓	✓

Table 1: Comparison of Network Types

#### 4.1. Visibility Networks

The visibility transformations from TS to complex networks are based on traditional visibility algorithms from computational geometry[21], associated with the natural ordering of the TS. In Table 1 we listed the algorithms that were utilised in this work.

The Natural Visibility Graph (NVG), originally introduced by Lacasa et al. [10], is based on the concept of visibility. In the NVG, each data point in the TS is treated as a vertical bar whose height corresponds to its value. Two points are connected if the line of sight between them is not obstructed by any intermediate data point. This means that there is a direct line of sight between the bars without any interception. Expressed mathematically: If any two points  $(t_i, s_i)$  and  $(t_j, s_j)$  have visibility, the following condition applies to every point  $(t_k, s_k)$  in between:

$$s_k < s_i + \frac{(s_j - s_i)(t_k - t_i)}{(t_j - t_i)}, \quad i < k < j$$

where:  $t_i, t_j$  and  $t_k$  are the time coordinates of the points, while  $s_i, s_j$  and  $s_k$  are the TS values at these specific time coordinates. The created edges  $e$  are stored in an adjacency matrix  $A^{NVG}$ . The NVG algorithm is easy to implement and has quadratic complexity  $O(S^2)$ [20] in terms of computational complexity. However, the NVG algorithm has two disadvantages, as it does not take into account the effect of uneven TS sampling and does not capture TS changes when the values are negative.

To overcome these disadvantages, a variation of NVG called the Weighted Dual Perspective Visibility Graph (WDPVG) was proposed by Zheng et al.[9]. According to the authors, the WDPVG method deals with uneven sampling in the time series by explicitly assigning weights to edges between nodes based on metrics such as Euclidean distance, tangent of the viewing angle, or actual time differences between connected points. Additionally, WDPVG captures both peaks and troughs of the time series, by incorporating a dual perspective, which is achieved by combining the NVG with its reflected counterpart. To compute the reflected perspective of the NVG (RPNVG), the time series is inverted by mirroring its values on the time axis, resulting in a new series  $S'_{1 \times N} = -S_{1 \times N}$ . A NVG is then constructed on this inverted series, resulting in an additional adjacency matrix  $A_{RPNVG}$ , which adds new edges  $e_{i,j}$ .

The final adjacency matrix for WDPVG,  $A_{WDPVG}$ , is created by combining the original NVG matrix and the RPNVG matrix using the rule:

$$A_{WDPVG_{i,j}} = \max(A_{NVG_{i,j}}, A_{RPNVG_{i,j}})$$

The resulting graph  $G = (V, E)$  is defined by the nodes  $v_n \in V$ , representing each measurement  $s_N$  in the time series, and the edges  $e_{i,j} \in E$ , stored in the adjacency matrix  $A_{WDPVG}$ .

Another version of the VG proposed by Luque et al.[11] is called the Horizontal Visibility Graph (HVG). Here, the visibility between two points is determined by a horizontal criterion. In a HVG, two nodes  $v_i$  and  $v_j$  are connected if all intermediate nodes  $v_k$  satisfy the following condition:

$$s_i, s_j > s_k, \quad \forall k \in (i, j)$$

The HVG is simpler and computationally more efficient than the NVG. Because of the limiting visibility criteria it does not capture as much information as the NVG does, but it is suitable when a quick, lightweight graph representation is needed.

The Weighted [12] and Directed [22] Visibility Graphs are modifications of the core NVG or HVG, created by adding specific parameters to extend their functionality. By adding one of the two direction values: left to right (edge direction go from left to right according to the series temporal axis, which preserves the natural, temporal order of TSs) or top to bottom (edge directions go from top to bottom according to the value axis, focusing on magnitude differences between data points), we obtain a directed graph. Additionally, each edge in the graph going from one point to another can be associated with a feature vector or weight, denoted as  $w_{ij}$ . The 'weighted' parameter can take one of the following values: Euclidean distance, squared Euclidean distance, horizontal or vertical distance and their

absolute variants, slope, and absolute slope. The edges together with their weight values are stored in the adjacency matrix  $A$ .

#### 4.2. Transition Networks

Transition Networks can be seen in rows 9 to 11 in Table 1. They are created by converting sequences of data points from the TS into symbols (states), and mapping the symbols and transitions between them into nodes and edges, respectively. The construction of this type of network involves two steps. First, the TS is partitioned into  $k$  symbols (or states)  $q = \{q_1, q_2, \dots, q_k\}$  based on a chosen strategy, such as quantile partitioning or phase space reconstruction. Each data point  $s_i$  in the TS  $\mathbf{S} = \{s_1, s_2, \dots, s_N\}$  is mapped to a symbol  $q_j$  using a partitioning function:

$$q_j = f(s_i), \quad f : \mathbb{R} \rightarrow Q$$

Here,  $f(s_i)$  assigns a symbol to each data point based on its value. As summarized in Table 1, these networks are typically directed and weighted, with the edges capturing the frequency of transitions between the states, and by that the resulting network represents the dynamics of the TS. The corresponding adjacency matrix is a Markov transition field (MTF) matrix  $A_{\text{MTF}}$ , given by :

$$A_{\text{MTF},i,j} = \begin{cases} A_{s_i,s_j} & \text{if } i \leq j, \\ 0 & \text{otherwise} \end{cases}$$

where  $A_{s_i,s_j}$  represent the probability of transitioning from state  $q_j$  to state  $q_i$ , and  $i$  and  $j$  are indices of the time series data points, mapped to their corresponding states  $q$ .

The computational complexity of the MTF increases quadratically with the length of the TS. Since the average length of the TS data in our benchmark datasets exceeds 3000, the application of the MTF becomes prohibitively expensive. Three main examples of this network type are Quantile Graphs[23], Ordinal Partition Transition Networks (OPTN) and Coarse-Grained Phase Space Graphs(CGPS).

#### 4.3. Proximity Networks

The utilised type of the Proximity Network can be seen in the last row in Table 1. The proximity concept, on which these networks are based on, means that the measure of distance  $d(s_i, s_j)$  or similarity (correlation)  $r(s_i, s_j)$  is used to calculate the distance between the points in the TS incorporated in the multidimensional phase space. Nodes in this network represent the states of the TS, and edges are established based on the chosen distance or similarity metric. For example, the utilised k-NN network as shown in Table 1, has edges based on the measure of distance between the nodes. The ability to connect different nodes based on proximity measures allows capturing meaningful information about the topology of dynamical systems, enabling to identify different regimes or patterns along the series.[24]. The adjacency matrix for this type of network can, in general, be written as:

$$A_{i,j} = \begin{cases} 1 & \text{if } d(s_i, s_j) \leq \epsilon \text{ or } r(s_i, s_j) \geq \alpha \text{ (binary matrix),} \\ w_{i,j} & \text{if proximity measure is used and weighting is applied,} \\ 0 & \text{otherwise.} \end{cases}$$

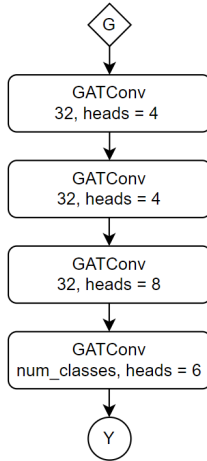
Proximity networks include cycle networks[25][26], correlation[27] and recurrence networks[28].

## 5. Proposed segmentation model

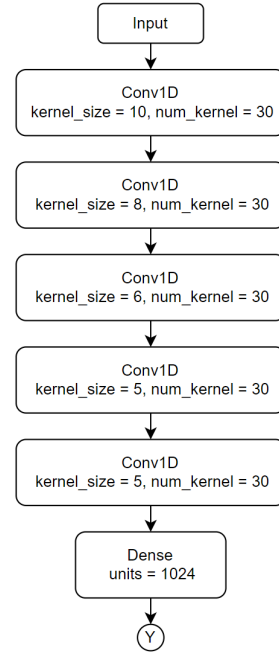
In this section we describe our proposed model. As described in Section 3, our goal is a point-wise classification task, where a class must be assigned to each point in the TS. After transforming the TS into a graph representation, as described in Section 4, our point-wise classification task converts into a node classification task. In other words, each node in the graph corresponds to a time point, and we predict a label for each node. Formally, we define our prediction model as a function  $\Phi$ , which transforms the input data  $G$  to the set of target classes  $Y_{1 \times N}$ :

$$\Phi : G \rightarrow Y_{1 \times N}$$

### 5.1. Proposed GNN model



(a) Proposed GNN network architecture



(b) Baseline sequence2point network architecture

Figure 2: Comparison of network architectures for TS segmentation

To realize the function  $F_G()$ , from Eq.3 to predict target classes from the transformed graph data denoted as  $G$ , a Graph Neural Network (GNN) was designed based on the Graph Attention Networks (GAT)[29]. The main advantage of GAT is a self-attention mechanism on node features that significantly improves classification performance for node classification tasks. This allows the model to calculate attention scores between nodes and their neighbors, which determine the influence each neighboring node has when updating a node’s feature representation. Unlike traditional GNNs, which aggregate information from all neighbors equally, GAT learns to focus on the most relevant ones, improving the accuracy of its predictions.

As shown in Figure 2a, the proposed architecture consists of 4 GAT layers. The first 3 layers have 32 neurons each but vary in the number of self-attention heads. The first two layers employ 4 attention heads, while the third layer employs 8 heads. The fourth layer has as many neurons as there are target classes and operates with 6 self-attention heads. We designed the architecture empirically by searching for the best ratio between the models complexity and performance. The configuration of the layers, filters, and attention heads was optimized through a grid search process, aiming to achieve the optimal ratio between model complexity and performance. The output of the final layer is passed to the output layer  $Y$ . For each of the nodes the network returns the probability of it being in one of the TS segments. All hidden layers use the Exponential Linear Unit (ELU) function for activation, while the final layer uses a softmax function. The ELU activation function handles the negative input values from the TS, while also contributing to the model convergence and accuracy.

## 5.2. Selected baseline model

SotA DL TSS approaches, such as seq2seq [8], focus on sliding window methods, limiting granularity due to their fixed size. To overcome this and allow fair comparison to our proposed dense labeling approach, our baseline is based on the sequence2point (seq2point) DL model [30], which is an adaptation of seq2seq. This version avoids window-based segmentation constraints by predicting a single midpoint element of a window.

The architecture of the baseline DL model is depicted in Figure 2b. The input TS window is fed into five consecutive one dimensional convolutional layers. First layer consists of 30 kernels of size 10, second of 30 kernels of size 8, third of 40 kernels of size 6, followed by two layers consisting of 50 kernels of size 5. The output of the last convolutional layer is fed into a Fully connected or Dense layer consisting of 1024 node units, which is then connected to the output layer of size  $Y$ , where the softmax activation function is applied and the classification is made. Size of the  $Y$  depends on the number of different classes present in the used dataset. All convolutional layers have a stride of 1, while both convolutional and Dense layers employ the Rectified Linear Units (ReLU) activation function.

## 6. Methodology and experimental details:

To outline the specifics of our work, first we explain the process of dataset preparation and then show the details of model training and evaluation processes.

### 6.1. Dataset

We validated our method using the TSSB dataset [14]. This dataset contains 75 annotated univariate TS with between 1 and 9 segments. Following common evaluation methodologies in TSS, we excluded TS containing only one segment, as they inherently lack change points and thus do not provide meaningful information about our method’s segmentation performance. Furthermore, TS containing duplicated segments were also discarded, since the dataset only contains the change point locations without the labels of each segment. As a result, our final dataset included 59 different TSSB datasets covering various domains, ensuring that our method is domain agnostic.

For our proposed method, each of the datasets was transformed into different graph representations as outlined in Section 4. For the seq2point baseline model, we applied a sliding window approach with a window length of 51 samples. Due to the limited length of certain TSSB datasets, this provided the best balance between the number of samples that could be used to train the model and the performance of the model. The center points of each window were labeled. The window was moved along the entire length of the TS dataset with a step of 1 so that the labels were assigned to all points. Due to the windowing process, the first and last 25 points of the TS had to be excluded to prevent loss of critical information.

### 6.2. Model training and evaluation

For training our proposed model for the node classification task, we utilized a standard node masking approach to split the dataset into training and testing sets with an 80:20 ratio. For each dataset within TSSB, we applied random node masking three separate times using different seeds. The model was then trained using only the nodes included in the training mask, and its performance was evaluated on the test nodes. A similar 80:20 split approach was used to train the baseline seq2point model, ensuring that both models follow the same data partitioning strategy. Each model was trained and tested five times with different random seeds, and the final performance results are reported as the average of these runs to account for variability in the random splits.

Given that our datasets are imbalanced, where the number of instances in different classes is not equal, we assigned weights to the classes during the training process. The weights were calculated based on the inverse proportion of each class in the dataset. By assigning higher weights to the minority classes and lower weights to the majority classes, the model is forced to pay more attention to the minority ones. Otherwise it gets higher penalties if miss-classifying them. The models were trained for 1500 epochs using batch size 1 to process the graph as a whole.

For evaluating performance, we relied on the standard F1 score for each class, calculated as:  $F1 \text{ score} = \frac{2 \times \text{Precision} \times \text{Recall}}{\text{Precision} + \text{Recall}}$ , where:  $\text{Precision} = \frac{TP}{TP+FP}$ ,  $\text{Recall} = \frac{TP}{TP+FN}$ , and TP, FP and FN stand for true positives, false positives and false negatives.

### 6.3. Comparative Analysis of Training Sample Ratios

To further highlight the advantages of our proposed model over the baseline, especially in terms of performance and data efficiency, we conducted an additional experiment in which we analyze the effects of different train-test split

ratios. The experiment was conducted utilizing random shuffle splits across a range of ratios from 10:90 to 90:10 with a step of 10. At each split, the experiments were repeated three times. The experiment highlights one of the main advantages of our approach: it achieves higher model performance with considerably less training data, as described in Section 7.3.

## 7. Results

In this section, we evaluate the performance of our proposed TSS approach. The details of the experimental setup used to obtain the results are described in Section 6.

We start with a comparison of the baseline model with our proposed GAT model combined with the TS to graph transformations previously listed in Table 1. The utilized TSS methods were evaluated on the full set of 59 TSSB datasets, with the results visualized by boxplots in Figure 3. Each boxplot represents a specific combination of the proposed GAT model and a transformation. Different transformations are distinguished by color, with the color legend provided at the bottom of Figure 3.

Afterwards, we analyze how the models perform on datasets grouped by the number of segments. Figures 4-8 show the results for datasets containing between 2 and 7 segments and follow the same boxplot format as in Figure 3

At the end of the section, we explain the impact of different test-train split ratios on both the proposed and the baseline model.

### 7.1. Overall model performances

Figure 3 shows the overall performance of all implemented TSS methods across 59 univariate TSSB datasets. Each boxplot summarizes the distribution of performance scores for a given TS to graph transformation combined with the proposed GAT model, except for the first boxplot, which represents the baseline model. From left to right, the next 22 boxplots correspond to different VG transformations, followed by 5 boxplots for Transition networks and the last one for a Proximity network. The central line in each boxplot is the median, while the top and bottom edges mark the 75th and 25th percentiles, forming the interquartile range (IQR). The whiskers extend up to 1.5 times the IQR, and all points outside the whiskers are considered as outliers. In this context, higher medians and narrower boxes generally indicate stronger and more consistent performance. Of all the models evaluated, the WDPVG, the simple NVG and the weighted NVG variant with different edge weight initializations achieved the best results.

If we look at the first boxplot from the left in Figure 3, we see a moderate performance with a median F1 score of 0.93. The IQR extends roughly from 0.9 to 0.97, which is slightly wider and suggests that the baseline model is less stable and more sensitive to fluctuations in the dataset compared to stronger NVG-based approaches. There are notable outliers at around 0.6 and 0.45, indicating lower performance on certain datasets.

In contrast, the WDPVG method, second boxplot from the left in Figure 3, achieves the best overall performance compared to both the baseline and other TS to graph transformations. This is in line with our expectations outlined



Figure 3: Combined overall performance across all the datasets

in Section 4, where we discussed the advantages of the WDPVG transformation, including its ability to capture additional structural information through its dual perspective. The median F1 score is positioned very high, close to 0.98. Combined with the narrow IQR and short whiskers, this suggests both superior performance and greater stability. This indicates that the WDPVG transformation consistently captures the underlying patterns and change points across various datasets, which underlines its suitability as the best performing transformation in combination with the GAT model.

Comparing the undirected and unweighted NVG, shown in the third boxplot from the left in Figure 3 with the weighted NVG variants shown in boxplots 4-8, we observe a very similar overall performance. The median values across all variants are consistently above 0.9, with a similarly narrow IQR. This indicates that the topological or structural features have more influence on the segmentation process than the edge weights. Edges define the overall structure of the graph by connecting data points, while edge weights primarily influence how these relationships are interpreted rather than altering or influencing the topology itself.

Boxplots 9-16 in Figure 3 represent the NVG variants with assigned edge directions. the left to right orientation outperforms the top to bottom direction, which is aligning naturally with the sequential order of TS data. Furthermore, we see that all directed variants exhibit higher variability and a greater number of outliers than their undirected counterparts. This is because directionality constrains the way the nodes in the graph are connected. In undirected VGs, every node is equally visible in both directions, whereas directed VGs filter out certain connections. As a result, the model misses out on useful structural information.

Compared to the more successful NVG-based methods, the HVG variants listed in boxplots 17 to 23 from the left in Figure 3, exhibit a greater dispersion of performance scores and a higher number of outliers. This increased variability is not surprising, as the horizontal line of sight can oversimplify the relationships between data points, potentially overlooking important structural transitions. Consequently, the HVGs' median performance values often fall below those of the NVGs, approximately around the value 0.85, and their wider IQRs and long extending whiskers suggest less consistency across different datasets.

Finally, the MTF and proximity transformations, shown in boxplots 24 to 29 in Figure 3, resulted in a complex network representation that makes the detection of significant structures practically impossible in our TSS task. As illustrated in Figure 3, these transformations produce the lowest median values in their respective boxplots and have some of the widest IQRs compared to all other transformations. The probabilistic nature of these transformations not only captures the noise in the data, but also smooths out sudden changes or local fluctuations that are crucial for accurate segmentation [31].

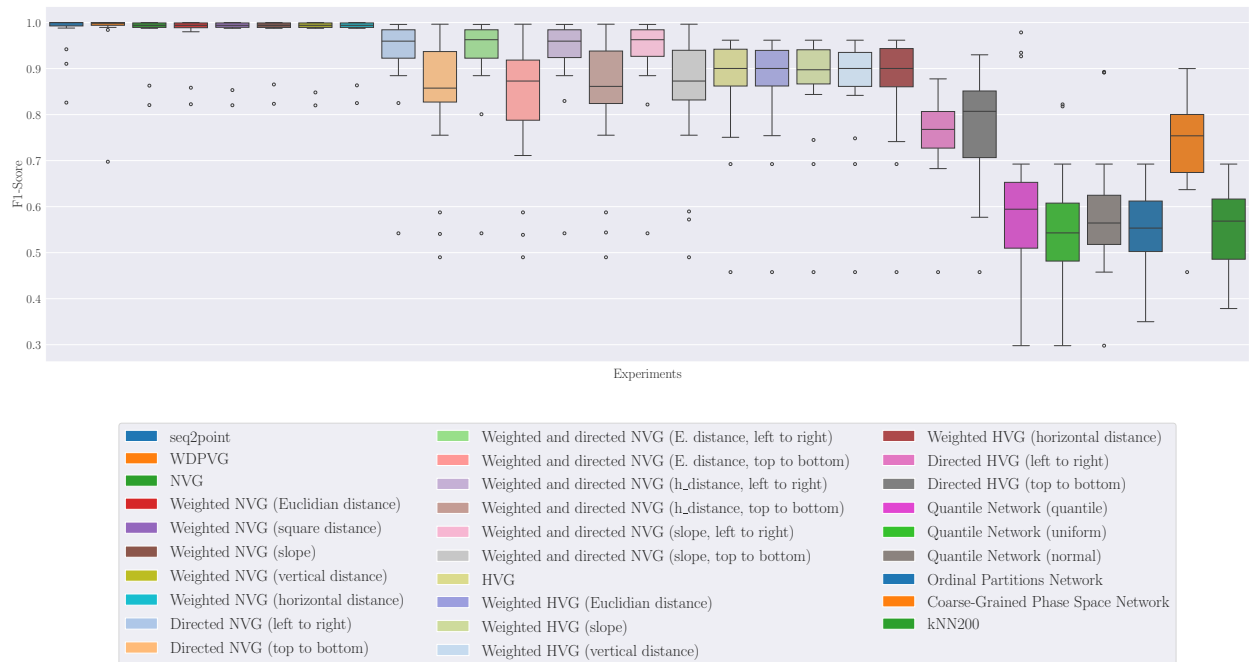


Figure 4: Boxplot summarizing the F1 score variability across various network architectures for 2 segment datasets.

## 7.2. Performance comparison based on number of segments

In this subsection, we compare the performance of our proposed WDPVG-based model with the baseline seq2point model across datasets with different number of segments. We specifically focus on the WDPVG, NVG, and baseline model, since NVG is foundational to WDPVG. Other models discussed previously have been analyzed in detail in Section 7.1.



Figure 5: Boxplot summarizing the F1 score variability across various network architectures for 3 segment datasets.

Figure 4 shows the results for 21 TSSB datasets with two segments. In this simpler segmentation task, all three models perform similarly, as shown by the tightly clustered boxplots with median F1 scores just below 1.0. The corresponding Table 3 (in the Appendix section) shows that the baseline model achieves a slight lead overall, but the difference is minimal, and both WDPVG and NVG remain highly competitive in this task.

As the complexity increases to datasets with three segments, the WDPVG-based model starts to outperform the baseline model significantly, as shown in Figure 5. WDPVG achieves a median F1 score of around 0.98 with a narrow IQR of 0.97–0.99, indicating stable performance. In contrast, the baseline’s median drops to around 0.91, with a wider IQR (0.85–0.93), indicating less stability. NVG maintains its strong performance with the median value of approximately 0.95, placing it between WDPVG and baseline.

In Figure 6, the results for four segment datasets show the advantage of WDPVG even more clearly. The WDPVG model maintains its high performance with a median around 0.98 and an exceptionally low variability (IQR 0.97–0.985). The performance of the baseline model decreases, reaching a median value of around 0.9 with greater variability (IQR 0.87–0.94). NVG remains competitive, with a median performance close to 0.97, but slightly greater variability compared to WDPVG.

For datasets with five segments, WDPVG continues to outperform the competition, as shown in Figure 7. Again, the median F1 score is 0.98 and variability is minimal (IQR 0.965–0.985). NVG follows close behind and continues to perform strongly with a median score of 0.96, albeit with slightly greater variability. The baseline model, although slightly improved compared to the simpler scenarios, still lags behind (median approximately 0.94) and shows higher

variability, including outliers around 0.85.

Finally, in the most complex scenarios with six or seven segments, illustrated in Figure 8, WDPVG shows exceptional performance, achieving a median of around 0.985 and consistently low variability (IQR 0.97–0.99). NVG also shows strong performance, though with slightly lower median values (0.97) and slightly higher variability. Conversely, the baseline model lags significantly behind both methods with a median of 0.91 and greater variability (IQR 0.87–0.93). These results suggest that the WDPVG is particularly effective for complex segmentation tasks, highlighting its ability to capture key structural dependencies within the data.

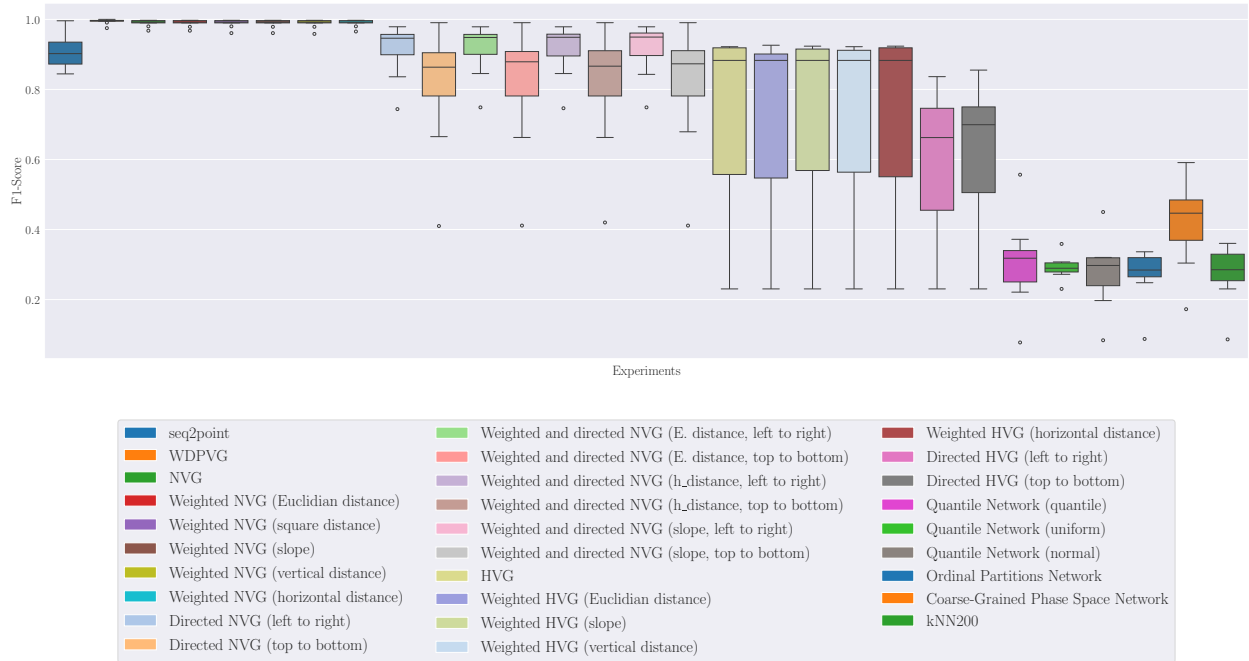


Figure 6: Boxplot summarizing the F1 score variability across various network architectures for 4 segment datasets.

### 7.3. Analysis of Training Sample Ratios on Model Performance

To evaluate the effect of the number of training samples on classification performance, we compared the proposed WDPVG-based model and the baseline model using the methodology described in Section 6. Figure 9 illustrates how the ratio of training to testing data impacts the model’s performance. The graph displays the average weighted F1 scores across all 59 datasets. As expected, the F1 scores for both the proposed and baseline models gradually improve as the proportion of training data increases. Also, this figure highlights the advantages of our approach. Even when using a fraction of only 10% of the available data for training, it achieves an impressive average F1 score of 0.95, significantly outperforming the baseline score of 0.73. This trend continues also for other ratios, which proves that our approach requires considerably less training data to achieve higher model performance, compared to the baseline.



Figure 7: Boxplot summarizing the F1 score variability across various network architectures for 5 segment datasets.



Figure 8: Boxplot summarizing the F1 score variability across various network architectures for 6 and 7 segment datasets.

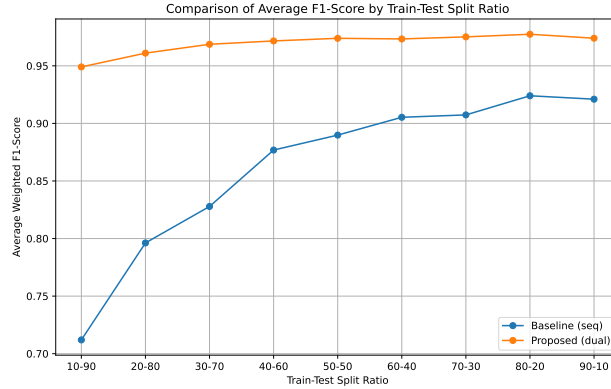


Figure 9: Impact of different train-test split ratios on the TSS model performance across TSSB datasets

Additionally, we compared the number of trainable parameters of the proposed and baseline model. As it can be seen in Table 2, our proposed model has  $\approx 10$  times less weights compared to the seq2point baseline, which means our proposed method is much less complex compared to the baseline model, and on average performs with a much higher F1 score across all the datasets.

Model	Number of trainable weights
Proposed model	$\approx 0.117M$
seq2point	$\approx 1.174M$

Table 2: Model trainable weights comparison

## 8. Conclusions

In this paper, we introduced a novel TSS approach that transforms time series data into graphs via the WDPVG and utilizes Graph Attention Networks (GAT) for segment classification. We also conducted an extensive study on various transformations of time series— into graphs — including simple and weighted visibility graphs as well as transition and proximity networks — and analyzed their strengths and limitations for TSS. Based on our findings, we conclude the following:

- Our proposed WDPVG consistently exhibits superior performance, achieving an average F1 score of 0.97 in 59 benchmark datasets. By capturing both peaks and troughs and addressing uneven sampling, WDPVG effectively preserves important structural information in time series.
- We validated the proposed method with the TSSB repository, which includes datasets from different domains such as gesture recognition, ECG recordings, and sensor-based measurements. The consistently high performance in these different contexts underlines the broad applicability of our approach.

- Our work demonstrates how transforming time series into graphs can improve a model’s ability to capture complex and wide-ranging relationships — particularly beneficial for multi-segment scenarios. By integrating graph representations with a Graph Attention Network, we achieve an F1 improvement of about 0.05 over a strong seq2point baseline.
- An important practical advantage lies in the data efficiency of our method. It requires significantly fewer labeled samples to converge while maintaining competitive accuracy. This makes the approach particularly attractive when working with large datasets that have limited labeled data.
- Experiments also show that the WDPVG exhibits high stability, even for dynamic datasets with potential noise and abrupt shifts. This resilience stems from the dual visibility perspective, which enriches the graph’s connectivity and improves the GNN’s ability to learn unique segment boundaries.

Overall, our study demonstrates that combining graph-based time-series transformations with GNN architectures can significantly improve TSS. By effectively capturing both the temporal and topological features of time series, our WDPVG and GAT approach not only consistently achieves higher segmentation accuracy, but also generalizes well across different domains. We anticipate that these findings will drive further research to develop advanced graph-based methods for various time series analysis tasks.

## Acknowledgements

This work was supported by the Slovenian Research Agency (P2-0016) and the European Commission NANCY project (No. 101096456).

## Author contributions statement

B.B., C.F. and I.K. conceived the experiments, I.K. conducted the experiments, B.B. and I.K. analysed the results. M.M. and C.F. provided funding. I.K. and B.B. wrote the original draft. All authors reviewed the manuscript.

## References

- [1] T. P. Carvalho, F. A. Soares, R. Vita, R. d. P. Francisco, J. P. Basto, S. G. Alcalá, A systematic literature review of machine learning methods applied to predictive maintenance, *Computers & Industrial Engineering* 137 (2019) 106024.
- [2] R. Qaddoura, A. M. Al-Zoubi, H. Faris, I. Almomani, A multi-layer classification approach for intrusion detection in iot networks based on deep learning, *Sensors* 21 (9) (2021) 2987.
- [3] S. Khan, T. Yairi, A review on the application of deep learning in system health management, *Mechanical Systems and Signal Processing* 107 (2018) 241–265.
- [4] F. A. Gers, J. Schmidhuber, F. Cummins, Learning to forget: Continual prediction with lstm, *Neural computation* 12 (10) (2000) 2451–2471.
- [5] S. Aghabozorgi, A. S. Shirkhorshidi, T. Y. Wah, Time-series clustering—a decade review, *Information systems* 53 (2015) 16–38.

- [6] I. Lebedev, B. Rzyev, Segmentation of data when analyzing the state of telecommunication systems, *Indonesian Journal of Electrical Engineering and Computer Science* 29 (3) (2023) 1473–1479.
- [7] M. Perslev, M. Jensen, S. Darkner, P. J. Jennum, C. Igel, U-time: A fully convolutional network for time series segmentation applied to sleep staging, *Advances in neural information processing systems* 32 (2019).
- [8] H. Phan, F. Andreotti, N. Cooray, O. Y. Chén, M. De Vos, Seqsleepnet: End-to-end hierarchical recurrent neural network for sequence-to-sequence automatic sleep staging, *IEEE Transactions on Neural Systems and Rehabilitation Engineering* 27 (3) (2019) 400–410. doi: 10.1109/TNSRE.2019.2896659.
- [9] M. Zheng, S. Domanskyi, C. Piermarocchi, G. I. Mias, Visibility graph based temporal community detection with applications in biological time series, *Scientific reports* 11 (1) (2021) 5623.
- [10] L. Lacasa, B. Luque, F. Ballesteros, J. Luque, J. C. Nuno, From time series to complex networks: The visibility graph, *Proceedings of the National Academy of Sciences* 105 (13) (2008) 4972–4975.
- [11] B. Luque, L. Lacasa, F. Ballesteros, J. Luque, Horizontal visibility graphs: Exact results for random time series, *Physical Review E Statistical, Nonlinear, and Soft Matter Physics*.
- [12] S. Supriya, S. Siuly, H. Wang, J. Cao, Y. Zhang, Weighted visibility graph with complex network features in the detection of epilepsy, *IEEE access* 4 (2016) 6554–6566.
- [13] W. Shen, Z. Peng, X. Wang, H. Wang, J. Cen, D. Jiang, L. Xie, X. Yang, Q. Tian, A survey on label-efficient deep image segmentation: Bridging the gap between weak supervision and dense prediction, *IEEE transactions on pattern analysis and machine intelligence* 45 (8) (2023) 9284–9305.
- [14] A. Ermshaus, P. Schäfer, U. Leser, Clasp: parameter-free time series segmentation, *Data Mining and Knowledge Discovery* 37 (3) (2023) 1262–1300.
- [15] S. N. A. M. Arif, M. F. M. Mohsin, A. A. Bakar, A. R. Hamdan, S. M. S. Abdullah, Change point analysis: a statistical approach to detect potential abrupt change, *Jurnal Teknologi* 79 (5) (2017).
- [16] S. Gharghabi, Y. Ding, C.-C. M. Yeh, K. Kamgar, L. Ulanova, E. Keogh, Matrix profile viii: domain agnostic online semantic segmentation at superhuman performance levels, in: *2017 IEEE international conference on data mining (ICDM)*, IEEE, 2017, pp. 117–126.
- [17] S. Gaugel, M. Reichert, Prectime: A deep learning architecture for precise time series segmentation in industrial manufacturing operations, *Engineering Applications of Artificial Intelligence* 122 (2023) 106078.
- [18] T. De Ryck, M. De Vos, A. Bertrand, Change point detection in time series data using autoencoders with a time-invariant representation, *IEEE Transactions on Signal Processing* 69 (2021) 3513–3524.
- [19] P. Veličković, G. Cucurull, A. Casanova, A. Romero, P. Liò, Y. Bengio, Graph Attention Networks, *International Conference on Learning Representations* (2018).  
URL <https://openreview.net/forum?id=rJXMpikCZ>
- [20] V. F. Silva, M. E. Silva, P. Ribeiro, F. Silva, Time series analysis via network science: Concepts and algorithms, *Wiley Interdisciplinary Reviews: Data Mining and Knowledge Discovery* 11 (3) (2021) e1404.
- [21] S. K. Ghosh, *Visibility algorithms in the plane*, Cambridge university press, 2007.
- [22] L. Lacasa, A. Nunez, É. Roldán, J. M. Parrondo, B. Luque, Time series irreversibility: a visibility graph approach, *The European Physical Journal B* 85 (2012) 1–11.
- [23] A. S. L. de Oliveira Campanharo, F. M. Ramos, Quantile graphs for the characterization of chaotic dynamics in time series, in: *2015 Third World Conference on Complex Systems (WCCS)*, Ieee, 2015, pp. 1–4.
- [24] R. V. Donner, M. Small, J. F. Donges, N. Marwan, Y. Zou, R. Xiang, J. Kurths, Recurrence-based time series analysis by means of complex network methods, *International Journal of Bifurcation and Chaos* 21 (04) (2011) 1019–1046.
- [25] J. Zhang, M. Small, Complex network from pseudoperiodic time series: Topology versus dynamics, *Physical review letters* 96 (23) (2006) 238701.
- [26] J. Zhang, X. Luo, M. Small, Detecting chaos in pseudoperiodic time series without embedding, *Physical Review E Statistical, Nonlinear, and*

Soft Matter Physics 73 (1) (2006) 016216.

- [27] Y. Yang, H. Yang, Complex network-based time series analysis, *Physica A: Statistical Mechanics and its Applications* 387 (5-6) (2008) 1381–1386.
- [28] N. Marwan, A historical review of recurrence plots, *The European Physical Journal Special Topics* 164 (1) (2008) 3–12.
- [29] P. Veličković, G. Cucurull, A. Casanova, A. Romero, P. Lio, Y. Bengio, Graph attention networks, arXiv preprint arXiv:1710.10903 (2017).
- [30] C. Zhang, M. Zhong, Z. Wang, N. Goddard, C. Sutton, Sequence-to-point learning with neural networks for non-intrusive load monitoring, in: *Proceedings of the AAAI conference on artificial intelligence*, Vol. 32, 2018.
- [31] Z. Wang, T. Oates, Encoding time series as images for visual inspection and classification using tiled convolutional neural networks, in: *Workshops at the twenty-ninth AAAI conference on artificial intelligence*, 2015.

## APPENDIX

In this section, we have summarized the detailed performance results in Tables 2-6, where each table groups the datasets by the same number of classes or distinct segments. The first column shows the name of the dataset, while the remaining columns show the selected metrics for the trained models, more specifically the proposed WDPVG, the Weighted NVG (Euclidean distance) and the baseline model seq2point. The last row in each table shows the average values of these metrics for each subset of the dataset. As we can see in Table 3, the WDPVG and the NVG perform quite similarly, with the NVG winning or drawing in 10/21 records and the WDPVG achieves 6 draws. The baseline model performs best overall, winning or drawing in 15/21 datasets, demonstrating its capability in handling simpler segmentation tasks with 2 segments. Although the additional information provided by the Reflected Perspective NVG contributes to the high F1 score values of the WDPVG, it does not offer a clear advantage over the other two models.

Dataset (num. segm.)	Proposed method			NVG			seq2point		
	Prec.	Rec.	F1	Prec.	Rec.	F1	Prec.	Rec.	F1
ArrowHead (2)	0.997	0.997	0.997	1.000	1.000	<b>1.000</b>	1.000	1.000	<b>1.000</b>
Beef (2)	0.996	0.996	0.996	0.986	0.986	0.986	1.000	1.000	<b>1.000</b>
BeetleFly (2)	0.998	0.998	0.998	1.000	1.000	<b>1.000</b>	1.000	1.000	<b>1.000</b>
BirdChicken (2)	1.000	1.000	<b>1.000</b>	1.000	1.000	<b>1.000</b>	0.988	0.988	0.988
ChlorineConcentration (2)	0.682	0.682	0.682	0.838	0.838	0.838	0.917	0.910	<b>0.906</b>
Coffee (2)	0.980	0.980	0.980	0.980	0.980	0.980	0.994	0.994	<b>0.994</b>
Computers (2)	0.998	0.998	0.998	0.999	0.999	<b>0.999</b>	0.942	0.942	0.942
DistalPhalanxOutlineAgeGroup (2)	0.993	0.993	<b>0.993</b>	0.993	0.993	<b>0.993</b>	0.682	0.826	0.747
ECG200 (2)	0.992	0.992	0.992	0.991	0.991	0.991	1.000	1.000	<b>1.000</b>
ECGFiveDays (2)	1.000	1.000	<b>1.000</b>	0.993	0.993	0.993	1.000	1.000	<b>1.000</b>
GunPoint (2)	0.997	0.997	0.997	0.997	0.997	0.997	1.000	1.000	<b>1.000</b>
ItalyPowerDemand (2)	0.994	0.994	0.994	0.882	0.848	0.848	0.997	0.997	<b>0.997</b>
Lightning2 (2)	0.996	0.996	0.996	1.000	1.000	<b>1.000</b>	0.995	0.995	0.995
MedicalImages (2)	1.000	1.000	<b>1.000</b>	1.000	1.000	<b>1.000</b>	0.993	0.993	0.993
MoteStrain (2)	1.000	1.000	<b>1.000</b>	1.000	1.000	<b>1.000</b>	0.996	0.996	0.996
SonyAIBORobotSurface1 (2)	0.996	0.996	0.996	1.000	1.000	<b>1.000</b>	1.000	1.000	<b>1.000</b>
SonyAIBORobotSurface2 (2)	0.997	0.997	0.997	1.000	1.000	<b>1.000</b>	1.000	1.000	<b>1.000</b>
ToeSegmentation1 (2)	0.993	0.993	0.993	0.992	0.992	0.992	1.000	1.000	<b>1.000</b>
ToeSegmentation2 (2)	0.998	0.998	0.998	0.998	0.998	0.998	1.000	1.000	<b>1.000</b>
TwoLeadECG (2)	1.000	1.000	<b>1.000</b>	0.989	0.989	0.989	1.000	1.000	<b>1.000</b>
Yoga (2)	0.931	0.931	0.931	0.925	0.925	0.925	0.991	0.991	<b>0.991</b>
Mean	0.978	0.978	0.978	0.972	0.972	0.972	0.974	0.981	0.979
STD	0.072	0.072	0.072	0.049	0.049	0.049	0.069	0.042	0.056

Table 3: Classification results of proposed model compared to the baseline for 2 class segmentation.

Already in Tables 4 and 5, the WDPVG outperforms both NVG and the baseline by consistently achieving higher F1 scores across the majority of datasets.

Dataset (num. segm.)	Proposed method			NVG			seq2point		
	Prec.	Rec.	F1	Prec.	Rec.	F1	Prec.	Rec.	F1
CBF (3)	1.000	1.000	<b>1.000</b>	0.989	0.989	0.989	0.994	0.994	0.994
CinCECGTorso (3)	0.995	0.995	0.995	0.999	0.999	<b>0.999</b>	0.865	0.865	0.865
DiatomSizeReduction (3)	1.000	1.000	<b>1.000</b>	1.000	1.000	<b>1.000</b>	0.930	0.919	0.919
DistalPhalanxTW (3)	0.973	0.973	<b>0.973</b>	0.963	0.963	0.963	0.410	0.640	0.500
Haptics (3)	0.997	0.997	<b>0.997</b>	0.974	0.974	0.974	0.910	0.908	0.906
InlineSkate (3)	0.997	0.997	<b>0.997</b>	0.997	0.997	<b>0.997</b>	0.844	0.826	0.824
LargeKitchenAppliances (3)	0.996	0.996	<b>0.996</b>	0.996	0.996	<b>0.996</b>	0.938	0.936	0.936
Meat (3)	0.989	0.989	<b>0.989</b>	0.974	0.974	0.974	0.939	0.935	0.934
OliveOil (3)	0.235	0.485	0.317	0.235	0.485	0.317	0.559	0.508	<b>0.369</b>
OSULeaf (3)	0.986	0.986	0.986	0.993	0.993	0.993	0.995	0.995	<b>0.995</b>
ProximalPhalanxOutlineAgeGroup (3)	0.990	0.990	<b>0.990</b>	0.984	0.984	0.984	0.896	0.889	0.891
Trace (3)	0.999	0.999	<b>0.999</b>	0.996	0.996	0.996	0.925	0.916	0.914
WordSynonyms (3)	0.998	0.998	<b>0.998</b>	0.992	0.992	0.992	0.738	0.859	0.794
Mean	0.935	0.935	0.935	0.929	0.929	0.929	0.842	0.861	0.834
STD	0.202	0.202	0.202	0.209	0.209	0.209	0.168	0.134	0.181

Table 4: Classification results of proposed model compared to the baseline for 3 class segmentation.

Dataset (num. segm.)	Proposed method			NVG			seq2point		
	Prec.	Rec.	F1	Prec.	Rec.	F1	Prec.	Rec.	F1
Adiac (4)	0.996	0.996	0.996	1.000	1.000	<b>1.000</b>	0.742	0.845	0.786
Car (4)	0.993	0.993	<b>0.993</b>	0.993	0.993	<b>0.993</b>	0.882	0.872	0.868
FaceFour (4)	0.996	0.996	<b>0.996</b>	0.994	0.994	0.994	0.886	0.883	0.877
FiftyWords (4)	0.999	0.999	<b>0.999</b>	0.992	0.992	0.992	0.966	0.960	0.961
InsectWingbeatSound (4)	1.000	1.000	<b>1.000</b>	1.000	1.000	<b>1.000</b>	0.995	0.995	0.995
Mallat (4)	0.995	0.995	<b>0.995</b>	0.992	0.992	0.992	0.910	0.912	0.910
ProximalPhalanxTW (4)	0.950	0.950	0.950	0.966	0.966	<b>0.966</b>	0.737	0.844	0.786
SwedishLeaf (4)	0.998	0.998	0.998	1.000	1.000	<b>1.000</b>	0.936	0.934	0.935
Symbols (4)	1.000	1.000	<b>1.000</b>	1.000	1.000	<b>1.000</b>	0.917	0.902	0.896
Mean	0.992	0.992	0.992	0.993	0.993	0.993	0.890	0.905	0.890
STD	0.015	0.015	0.015	0.010	0.010	0.010	0.067	0.048	0.067

Table 5: Classification results of proposed model compared to the baseline for 4 class segmentation.

In Table 6, we observe that our method’s capabilities are limited on gesture recognition datasets (Cricket X, Y and Z, UWaveGestureLibraryAll, X, Z), where the baseline method has a clear advantage.

Dataset (num. segm.)	Proposed method			NVG			seq2point		
	Prec.	Rec.	F1	Prec.	Rec.	F1	Prec.	Rec.	F1
CricketX (5)	0.995	0.995	0.995	0.998	0.998	<b>0.998</b>	0.995	0.995	0.995
CricketY (5)	0.983	0.983	0.983	0.988	0.988	0.988	0.991	0.991	<b>0.991</b>
CricketZ (5)	0.991	0.991	0.991	0.983	0.983	0.983	0.996	0.996	<b>0.996</b>
Lightning7 (5)	0.998	0.998	<b>0.998</b>	0.997	0.997	0.997	0.827	0.829	0.825
ShapesAll (5)	0.999	0.999	<b>0.999</b>	0.997	0.997	0.997	0.992	0.992	0.992
SyntheticControl (5)	0.991	0.991	0.991	0.992	0.992	<b>0.992</b>	0.691	0.813	0.739
UWaveGestureLibraryAll (5)	0.973	0.973	0.973	0.965	0.965	0.965	0.994	0.994	<b>0.994</b>
UWaveGestureLibraryX (5)	0.977	0.977	0.977	0.987	0.987	0.987	0.991	0.991	<b>0.991</b>
UWaveGestureLibraryY (5)	0.981	0.981	<b>0.981</b>	0.975	0.975	0.975	0.962	0.960	0.959
UWaveGestureLibraryZ (5)	0.984	0.984	0.984	0.991	0.991	0.991	0.994	0.994	<b>0.994</b>
Mean	0.987	0.987	0.987	0.987	0.987	0.987	0.943	0.955	0.948
STD	0.008	0.008	0.008	0.010	0.010	0.010	0.097	0.068	0.085

Table 6: Classification results of proposed model compared to the baseline for 5 class segmentation.

Table 7 shows that our proposed method is particularly suitable for datasets with six or more segments. It consistently outperforms the seq2point baseline (except for FaceAll) and demonstrates its effectiveness in capturing complex structural dependencies.

Dataset (num. segm.)	Proposed method			NVG			seq2point		
	Prec.	Rec.	F1	Prec.	Rec.	F1	Prec.	Rec.	F1
NonInvasiveFetalECGThorax1 (6)	0.997	0.997	<b>0.997</b>	0.997	0.997	<b>0.997</b>	0.890	0.882	0.841
NonInvasiveFetalECGThorax2 (7)	0.992	0.992	0.992	0.995	0.995	<b>0.995</b>	0.947	0.943	0.942
FaceAll (7)	0.971	0.971	0.971	0.983	0.983	0.983	0.996	0.996	<b>0.996</b>
FacesUCR (7)	0.981	0.981	<b>0.981</b>	0.976	0.976	0.976	0.781	0.876	0.823
Fish (7)	0.974	0.974	<b>0.974</b>	0.972	0.972	0.972	0.911	0.907	0.904
Plane (7)	0.996	0.996	<b>0.996</b>	0.988	0.988	0.988	0.785	0.880	0.828
Mean	0.985	0.985	0.985	0.985	0.985	0.985	0.885	0.914	0.889
STD	0.010	0.010	0.010	0.009	0.009	0.009	0.079	0.043	0.064

Table 7: Classification results of proposed model compared to the baseline for 6 and 7 class segmentation.